Acta Crystallographica Section A
**Foundations and Advances**
ISSN 2053-2733

Received 12 September 2013
Accepted 19 December 2013

# Alternative approaches to onion-like icosahedral fullerenes

**A. Janner**

Theory of Condensed Matter, FNWI, Radboud University, Heyendaalseweg 135, NL-6525 AJ Nijmegen, The Netherlands. Correspondence e-mail: a.janner@science.ru.nl

The fullerenes of the $C_{60}$ series ($C_{60}$, $C_{240}$, $C_{540}$, $C_{960}$, $C_{1500}$, $C_{2160}$ *etc.*) form onion-like shells with icosahedral $I_h$ symmetry. Up to $C_{2160}$, their geometry has been optimized by Dunlap & Zope from computations according to the analytic density-functional theory and shown by Wardman to obey structural constraints derived from an affine-extended $I_h$ group. In this paper, these approaches are compared with models based on crystallographic scaling transformations. To start with, it is shown that the 56 symmetry-inequivalent computed carbon positions, approximated by the corresponding ones in the models, are mutually related by crystallographic scalings. This result is consistent with Wardman's remark that the affine-extension approach simultaneously models different shells of a carbon onion. From the regularities observed in the fullerene models derived from scaling, an icosahedral infinite $C_{60}$ onion molecule is defined, with shells consisting of all successive fullerenes of the $C_{60}$ series. The structural relations between the $C_{60}$ onion and graphite lead to a one-parameter model with the same Euclidean symmetry $P6_3mc$ as graphite and having a $c/a = \tau^2$ ratio, where $\tau = 1.618\ldots$ is the golden number. This ratio approximates (up to a 4% discrepancy) the value observed in graphite. A number of tables and figures illustrate successive steps of the present investigation.



## 1. Introduction

The symmetry approach to virus architecture discussed by J. P. Wardman in her PhD thesis (Wardman, 2012) is based on the molecular crystallography of icosahedral viruses, taking into account the structural constraints by the point arrays derived from affine-extended symmetry groups (see, in particular, Keef *et al.*, 2013; Janner, 2013, and references therein). In this PhD thesis Wardman also applies aspects of the theory to fullerenes. The name 'fullerenes' designates hollow carbon spheroids (Kroto *et al.*, 1985). As pointed out by Wardman, viruses are not the only multishell polyhedral structures with icosahedral symmetry.

Typical in a molecular crystallographic approach are indexed polygons and polyhedra, where the rational indices of the vertices correspond to points of lattices (of a suitable dimension) left invariant by the point group of the molecular system. Such an approach has been applied to axial-symmetric biomacromolecules, where the architectural elements are indexed enclosing forms. The idea that an icosahedral virus represents a special case of these molecules allowed the identification of various types of indexed enclosing forms in the multishells of the virus, which involves, in particular, an external capsid and a genome, leading to a classification alternative with respect to the seminal one of Caspar and Klug (Caspar & Klug, 1962; Janner, 2006; Keef & Twarock, 2009).

The correlation between various indexed forms has been expressed in terms of crystallographic scalings, where the scaling transformation, represented by invertible matrices with rational entries, allows one to relate vertices of the indexed forms having different radial distances from the molecular centre. These scalings play an analogous role as the affine extensions introduced by the York group. The mutual relations are not trivial and require further investigation.

The constraints imposed by indexed forms and by point arrays, respectively, to viruses (and to axial-symmetric proteins) are only loosely related to atomic positions because of the typical chain structure involved (polypeptides and RNA, in particular) and this fact is a handicap when one tries to relate the geometric structure to physical, chemical and biological properties.

In fullerenes the situation is more favourable because they are pure carbon structures. It is, therefore, not surprising to find an extended literature of articles devoted to this fundamental problem, whose interest is enhanced by possible nanotechnological applications (see, for example, Fleming *et al.*, 1992; Bühl & Hirsch, 2001; Dunlap & Zope, 2006; Calaminici *et al.*, 2012, and references therein).

The 1993 article of Chung and Sternberg is a classical example of how to calculate properties of the $C_{60}$ fullerene, the so-called buckyball (Kroto *et al.*, 1985), from various points of view: topology, symmetry, group theory, spectroscopy, graph theory (Chung & Sternberg, 1993). In a similar

spirit, the structure of the fullerenes considered in this paper is presented according to alternative approaches: topological, computational, affine-extended and scaling ones.

Denoting by ($V\,E\,F$) the number of vertices $V$, of edges $E$ and of faces $F$, the topology of a three-dimensional polyhedron implies the Euler formula

$$V - E + F = 2. \tag{1}$$

In the icosahedral fullerene each carbon atom is bound to three other C atoms, so that the polyhedron of the molecular skeleton is denoted as *trivalent*.

For trivalent polyhedra Euler deduced the additional relation:

$$\sum_n (6-n) f_n = 12, \tag{2}$$

where $f_n$ is the number of polygons with $n$ sides forming a face of the polyhedron. As a fullerene polyhedron consists of hexagons and pentagons, the above Euler relations imply (Chung & Sternberg, 1993)

$$E = 3V/2, \quad F = 2 + V/2, \quad f_5 = 12. \tag{3}$$

In particular for $C_{60}$ one has ($V\,E\,F$) = (60 90 32), with 20 hexagons and 12 pentagons.

A few general remarks and perspectives for future investigations conclude this paper.

## 2. Alternative approaches

The various approaches considered are all based on the point-group symmetry of the icosahedral fullerenes. The two groups $I = 235$ and $I_h = m\overline{3}\overline{5}$ of the icosahedral system (order 60 and 120) are the largest finite subgroups of the three-dimensional orthogonal group $SO(3)$ and $O(3)$, respectively. While $I$ is the point group of the icosahedral viruses, that of the icosahedral fullerenes is $I_h$.

The present analysis is based on the computational approach of Dunlap & Zope (2006) of the most stable fullerene onions $C_{240}$, $C_{540}$, $C_{960}$, $C_{1500}$ and $C_{2160}$ (Kroto & McKay, 1988), taking into account the experimental geometry of $C_{60}$ optimized by using analytic functional theory and orbital basis sets of the multi-electrons involved. The ground-state energy of various onions of this series has been calculated and compared with that of single cages (Maiti *et al.*, 1993).

The result is summarized in Table 1 of the Dunlap–Zope paper in terms of the coordinates (in Å) of $I_h$-inequivalent carbon atoms. These coordinates $x, y, z$ are expressed with respect to the orthonormal basis $e = \{e_1, e_2, e_3\}$ oriented along the icosahedral twofold axes. The orbits, generated by $I_h$ from the atomic positions indicated, are either of order 120 or of order 60. The elements of the orbits define the vertices of corresponding polyhedra with icosahedral symmetry. In the 60-order case, one of the coordinates is necessarily zero, because mirror-equivalent points coincide.

The other two approaches, based on the ideas of molecular crystallography, investigate the possibility of approximating the experimental or the computed geometric fullerene structure by carbon positions having integral (or more generally rational) indices, according to six-dimensional faithful integral representations of the icosahedral groups. The one-to-one correspondence between the three-dimensional coordinates $(x, y, z)$ and the set of rational indices $[h_1, h_2, h_3, h_4, h_5, h_6]$ follows from the relation between the orthonormal basis $e$ and the basis $a = \{a_1, a_2, \ldots, a_6\}$ of a $\mathbb{Z}$ module $\Lambda_{\rm ico}$ of dimension 3 and rank 6 given by

$$\begin{array}{lll} a_1 = a_0(e_1 + \tau e_3), & a_2 = a_0(\tau e_1 + e_2), & a_3 = a_0(\tau e_2 + e_3), \\ a_4 = a_0(-e_1 + \tau e_3), & a_5 = a_0(-\tau e_2 + e_3), & a_6 = a_0(\tau e_1 - e_2), \end{array} \tag{4}$$

where $a_0$ is the icosahedral lattice parameter and $\tau = (1 + 5^{1/2})/2$ the golden number. Both approaches make use of results derived from a symmetry characterization of icosahedral viruses (Janner, 2006, 2013; Keef & Twarock, 2009; Keef *et al.*, 2013).

In the first of these molecular crystallographic approaches, the restrictions imposed by affine extensions of the icosahedral group (in the present case $I_h$) are applied to fullerenes, as discussed in Wardman's PhD thesis (Wardman, 2012). The second one, which is the object of the present paper, makes use of crystallographic scaling transformations (Janner, 2006).

The scaling transformations considered are the product of fractional scaling of the coordinates $x, y, z$ along icosahedral twofold axes:

$$X_k x = kx, \quad Y_k y = ky, \quad Z_k z = kz, \tag{5}$$

for a fraction $k = m/n$. The corresponding six-dimensional invertible matrices in the icosahedral basis $a$, reported in Appendix $A$, are of the type already considered in equation (13) of Janner (2006) and transform positions with rational indices into ones also with rational indices.

The fullerenes mentioned above are here discussed, starting from the $C_{60}$ cluster.

## 3. The $C_{60}$ fullerene

The topological relations of equation (3) imply for the geometry of $C_{60}$ a polyhedron (60 90 32) with 60 vertices, 90 edges, 32 faces: two types of faces (20 hexagons and 12 pentagons) and two types of edges, 60 pentagonal (denoted as $e_{\rm pent}$), given by the sides of the pentagons, and 30 hexagonal ($e_{\rm hex}$), which are those of contiguous hexagons.

The carbon positions computed by Dunlap–Zope are generated by $I_h$ from

$$Q[0] = (x_0, y_0, 0) = (3.4785, 0.6991, 0.0000), \tag{6}$$

where $Q$ denotes the computed orbit (of order 60) with elements $Q[n]$, $n = 0, 1, 2, \ldots, 59$, numbered according to the successive icosahedral transformations, which in the present case are those of the point group $I$, because mirror-related elements coincide. It is convenient to fix once and for all the succession.[1]

[1] Adopted is the same succession of the icosahedral transformations, in the twofold orientation, indicated as BIOMT in the PDB file with code 1aym (Hadfield *et al.*, 1997) of the human rhinovirus 16.

As the ratio $x_0/y_0 = 4.9757$ of the two non-vanishing coordinates indicated in their paper is different from $3\tau = 4.8541$, the hexagonal and the pentagonal edges have a different length. In the conventional order mentioned above, one finds that the two positions $Q[17]$, $Q[2]$ delimit a pentagonal edge and $Q[17]$, $Q[40]$ a hexagonal one:

$$e_{\rm pent} = d(Q[17], Q[2]) = 1.451,$$
$$e_{\rm hex} = d(Q[17], Q[40]) = 1.398, \quad (7)$$

where $d$ denotes distance and the values are in Å.

The geometrical form of $C_{60}$ is a truncated icosahedron. In the ideal case all edges have equal length. The truncation can be obtained from an icosahedron by 1/3-scaling of one coordinate of its vertices. So, for example, from the position at $3(1, 0, \tau) = 3[100000]$ [see equation (4) with icosahedral lattice parameter $a_0 = 1$], one finds the position

$$X_{1/3}(3, 0, 3\tau) = (1, 0, 3\tau) = [200100] \quad (8)$$

and all other equivalent ones for the *standard form* of the $C_{60}$ polyhedron with edge length 2 (for $a_0 = 1$), as listed in Tables A.4 and A.5 of Wardman's PhD thesis. The *ideal* $C_{60}$ fullerene has the same set of indexed positions but with $a_0 = 0.7042$ Å, for coordinates in Å. In particular the orbit $A$ generated from the carbon position

$$A[0] = 0.7042(3\tau, 1, 0) = (3.4182, 0.7042, 0.0000) = [020001] \quad (9)$$

approximates the computed one $Q[0]$ indicated in equation (6).

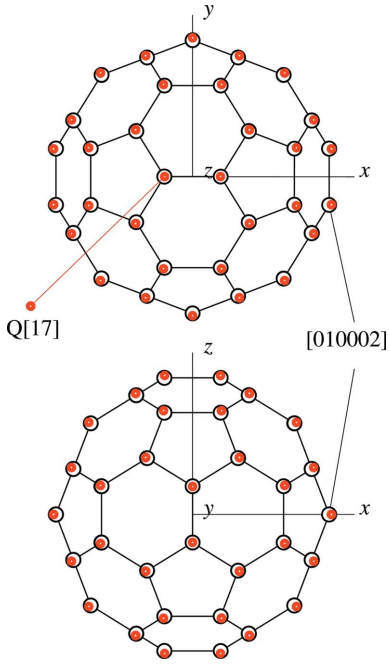


**Figure 1**
The $C_{60}$ fullerene (buckyball), oriented according to the icosahedral twofold axes, is shown along the $x$ axis (top view) and along the $y$ axis (bottom view). Compared are the indexed positions (black circles) with the positions (in red) of the orbit generated by $I_h$ from the coordinates indicated in Table 1 of Dunlap & Zope (2006).

**Table 1**
Orbital labelling of the onion fullerenes.

| | $I_h$ orbits | |
|---|---|---|
| Fullerenes | Order 120 | Order 60 |
| $C_{60}$ | | $Q_1$ |
| $C_{240}$ | $Q_2$ | $Q_3$, $Q_4$ |
| $C_{540}$ | $Q_8$, $Q_9$, $Q_{10}$ | $Q_5$, $Q_6$, $Q_7$ |
| $C_{960}$ | $Q_{11}$–$Q_{16}$ | $Q_{17}$–$Q_{20}$ |
| $C_{1500}$ | $Q_{21}$–$Q_{30}$ | $Q_{31}$–$Q_{35}$ |
| $C_{2160}$ | $Q_{36}$–$Q_{50}$ | $Q_{51}$–$Q_{56}$ |

One sees that it is precisely in the molecular crystallographic indexed approximation that one gets the ideal $C_{60}$ structure considered in the literature, with equal nearest-neighbour distance $2a_0$.

A view of $C_{60}$, shown in Fig. 1 along the $z$ axis (a twofold icosahedral direction), allows one to verify that the basis $a$ defined in equation (4) and denoted in Janner (2013) as 'ico1' is a compatible basis for $C_{60}$. (The concept of *compatibility* is discussed in the same paper, where alternative icosahedral bases are considered there in Table 6 and illustrated in Figs. 6 and 7.)

One distinguishes accordingly two indexed $C_{60}$ polyhedra generated from [210000] in the basis *ico1*: the *standard* $C_{60}$ for the icosahedral parameter $a_0 = 1$ and the *ideal* $C_{60}$ for $a_0 = 0.7042$ Å. The ideal one approximates the *computed* $C_{60}$, generated from $Q[0]$, which corresponds to the experimentally observed $C_{60}$ carbon fullerene.

## 4. The computed onion of the icosahedral fullerenes $C_{60}$, $C_{240}$, $C_{540}$, $C_{960}$, $C_{1500}$, $C_{2160}$

The computed carbon positions (with coordinates in Å) considered in this article are those listed in Table 1 of Dunlap & Zope (2006). The point group $I_h$ generates from these positions the various orbits, whose elements define the polyhedral vertices of the fullerenes listed above.

To allow comparison between the alternative approaches considered, it is convenient to label these positions (and the corresponding orbits) in the same sequential order as the one adopted in Table 1 of Dunlap and Zope.

In particular, the first orbit $Q_1$, of order 60, generated by $Q_1[0] = (3.4785, 0.6991, 0.0000)$ (denoted by $Q$ in the previous section) is the one of the computed $C_{60}$. The orbits $Q_2$ (of order 120), $Q_3$ and $Q_4$ (of order 60) are those of the fullerene $C_{240}$ and the last orbit considered is $Q_{56}$, generated by $Q_{56}[0] = (11.3039, 0.0000, 20.5910)$, of $C_{2160}$.

Table 1 summarizes the labelling of the orbits according to the list of positions given in Table 1 of Dunlap and Zope. All fullerenes considered are truncated icosahedra with 12 pentagonal and 20 hexagonal faces.

## 5. The $C_{60}$ series from $I_h$ affine extensions

As already mentioned, in the PhD work of Wardman (2012) the affine-extension method of the York group (see Keef *et al.*, 2013) is applied to fullerene models in a standard repre-

**Table 2**
Model of $C_{240}$ onion fullerene according to the affine-extended point arrays approach (Wardman, 2012).

| No. | Radius ($a_0 = 1$) | Orbit order | Affine-extended generator (first-order translation *3T5*) | Dunlap & Zope (2006) generator |
|---|---|---|---|---|
| 3 | 2.0000 | 30 | [1,$\bar{1}$,0,0,0,0] | |
| 7 | 4.0000 | 30 | [2,0,$\bar{2}$,0,0,0] | |
| 1 | 4.9559 | 60 | [0,$\bar{2}$,0,0,0,$\bar{1}$] | |
| 5 | 5.2915 | 120 | [3,0,0,$\bar{2}$,$\bar{1}$,0] | |
| 9 | 6.8861 | 120 | [3,0,0,$\bar{2}$,0,1] | |
| 4 | 8.1749 | 120 | [3,0,2,0,0,$\bar{1}$] | |
| 2 | 9.2867 | 120 | [3,0,1,2,0,0] | $Q_2$ |
| 6 | 9.9119 | 60 | [4,0,0,0,0,2] | $Q_3$ |
| 8 | 10.4997 | 60 | [5,0,1,0,0,0] | $Q_4$ |

sentation, in particular to elements of the $C_{60}$ series with shells of onion-like molecular structures composed of the fullerenes $C_{60}$, $C_{240}$, $C_{540}$, $C_{1500}$, $C_{2160}$, $C_{2940}$ (Kroto & McKay, 1988; Terrones *et al.*, 2002).

The aim of the present paper is not to give a full derivation of the results mentioned in Wardman (2012), but only to characterize her approach in comparison with alternative ones. Therefore the method is illustrated by the $C_{240}$ and $C_{540}$ shells only.

The start configuration is the standard $C_{60}$ polyhedron, whose 60 vertices are listed in Tables A.4 and A.5 of Wardman's thesis. Then, among the admissible translations given in Tables A.9 and A.10, Wardman found that the only relevant one for the $C_{60}$ series is along a fivefold axis with multiplier 3, indicated as 45 in the list of the point arrays of Table A.10. In the standard representation this translation, denoted *3T5*, can be chosen pointing from the origin to the indexed position [300000].

To begin with, the point group $I_h$ is applied to the start configuration translated by *3T5*. This gives rise to the nine orbits listed in Table 2. Among these orbits, three are the ones defining the standard $C_{240}$ polyhedron: one of order 120 and two of order 60. The identification indicated in Table 2 has here been obtained by comparison with the orbits $Q_2$, $Q_3$, $Q_4$ computed by Dunlap and Zope, as illustrated in Fig. 2. Repeating the procedure a second time by applying the same translation again, one then gets 46 inequivalent orbits and the six ones of the standard $C_{540}$ configuration, as indicated in Table 3. This concludes the present illustration of the affine-extended approach. As mentioned in Wardman's thesis on page 144, the subsequent shells can be derived in a similar way. Relevant is her remark that the procedure simultaneously models different shells of a carbon onion.

## 6. Crystallographic scalings applied to icosahedral fullerenes

The goal of the following alternative approach, the same as that of the previous one based on affine-extended point arrays, is to find the integral indexed positions which define the generators of fullerenes belonging to the $C_{60}$ series.

**Table 3**
Model of the fullerene $C_{540}$ according to the affine-extended point arrays approach (Wardman, 2012), leading to 46 $I_h$-inequivalent orbits.

| No. | Radius ($a_0 = 1$) | Orbit order | Affine-extended generator (first-order translation *3T5*) | Dunlap & Zope (2006) generator |
|---|---|---|---|---|
| 19 | 1.5209 | 60 | [3,$\bar{3}$,0,$\bar{2}$,$\bar{1}$,0] | |
| 31 | 2.0000 | 30 | [$\bar{1}$,0,0,0,1,0] | |
| ... | ... | ... | ... | ... |
| 17 | 8.9431 | 120 | [3,0,3,$\bar{2}$,$\bar{1}$,0] | |
| 5 | 8.9431 | 120 | [3,1,0,$\bar{3}$,$\bar{2}$,0] | |
| 23 | 9.1955 | 120 | [3,0,$\bar{5}$,$\bar{1}$,0,0] | $Q_9$ |
| 4 | 9.2868 | 120 | [0,0,1,3,0,$\bar{2}$] | |
| 42 | 9.3482 | 60 | [2,$\bar{2}$,0,3,0,0] | |
| ... | ... | ... | ... | ... |
| 37 | 13.1996 | 120 | [6,0,$\bar{1}$,0,0,2] | |
| 14 | 13.4773 | 120 | [5,1,0,0,3,0] | |
| 24 | 13.7497 | 120 | [4,2,0,0,0,3] | $Q_{10}$ |
| 1 | 14.1797 | 120 | [3,0,0,5,1,0] | |
| 34 | 14.5963 | 60 | [4,0,0,0,0,5] | $Q_6$ |
| 44 | 14.5964 | 120 | [6,0,0,0,2,1] | $Q_8$ |
| 46 | 15.3969 | 60 | [7,2,0,0,0,0] | $Q_5$ |
| 45 | 16.1575 | 60 | [8,1,0,0,0,0] | $Q_7$ |

The general philosophy, however, is quite different, not only because it is based on crystallographic scalings instead of affine extensions, but also because it starts from given experimental data or, as in the present case, from the computed ones by Dunlap and Zope, in order to determine the integral indices of the positions which approximate the given structure. One then extracts generic laws from the solutions found for the various shells. Typical in this process of approximating a three-dimensional position by a set of six integral indices is that one normally finds many nearly good solutions. 'Nearly good' is a solution which is quite acceptable

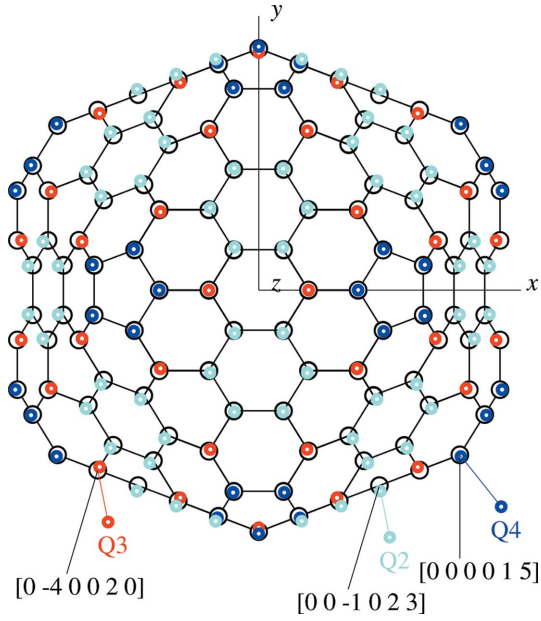


**Figure 2**
Model of the $C_{240}$ fullerene with positions (black circles) indexed according to the affine-extended point arrays identified by Wardman (2012) compared with the fitted orbits $Q_2$ (cyan), $Q_3$ (red) and $Q_4$ (blue) computed by Dunlap & Zope (2006) (see Table 2).

**Table 4**
Crystallographic scalings along the $x, y, z$ axes relating the $C_{60}$ positions $A_1[1] = [2, 0, 0, 1, 0, 0] = (1, 0, 3\tau)$ and $A_1[9] = [0, 2, 0, 0, 0, 1] = (3\tau, 1, 0)$ to order-60 positions of the shells $C_{240}$, $C_{540}$, $C_{960}$, $C_{1500}$, $C_{2160}$ (for $a_0 = 1$).

| Shell | Orbit | Scaling relation | Indexed position |
|---|---|---|---|
| $C_{240}$ | $A_3$ | $X_2Y_2A_1[9]$ | [0,4,0,0,0,2] |
| | $A_4$ | $X_2Y_4A_1[9]$ | [0,5,0,0,0,1] |
| $C_{540}$ | $A_5$ | $X_3Y_5A_1[9]$ | [0,7,0,0,0,2] |
| | $A_6$ | $X_3A_1[9]$ | [0,5,0,0,0,4] |
| | $A_7$ | $X_3Y_7A_1[9]$ | [0,8,0,0,0,1] |
| $C_{960}$ | $A_{17}$ | $X_2Z_4A_1[1]$ | [7,0,0,5,0,0] |
| | $A_{18}$ | $X_4Z_4A_1[1]$ | [8,0,0,4,0,0] |
| | $A_{19}$ | $X_{10}Z_4A_1[1]$ | [11,0,0,1,0,0] |
| | $A_{20}$ | $X_8Z_4A_1[1]$ | [10,0,0,2,0,0] |
| $C_{1500}$ | $A_{31}$ | $X_7Z_5A_1[1]$ | [11,0,0,4,0,0] |
| | $A_{32}$ | $X_5Z_5A_1[1]$ | [10,0,0,5,0,0] |
| | $A_{33}$ | $X_{11}Z_5A_1[1]$ | [13,0,0,2,0,0] |
| | $A_{34}$ | $X_{13}Z_5A_1[1]$ | [14,0,0,1,0,0] |
| | $A_{35}$ | $Z_5A_1[1]$ | [8,0,0,7,0,0] |
| $C_{2160}$ | $A_{51}$ | $X_2Z_6A_1[1]$ | [10,0,0,8,0,0] |
| | $A_{52}$ | $X_4Z_6A_1[1]$ | [11,0,0,7,0,0] |
| | $A_{53}$ | $X_{10}Z_6A_1[1]$ | [14,0,0,4,0,0] |
| | $A_{54}$ | $X_8Z_6A_1[1]$ | [13,0,0,5,0,0] |
| | $A_{55}$ | $X_{14}Z_6A_1[1]$ | [16,0,0,2,0,0] |
| | $A_{56}$ | $X_{16}Z_6A_1[1]$ | [17,0,0,1,0,0] |

from the numerical point of view, but misses essential global properties needed for the characterization of the expected relevant architectural elements, as is indeed the case for the ideal $C_{60}$ structure discussed in §3.

From the practical point of view, it is convenient to restrict, at first, the considerations to the orbits of order 60 (because this involves positions with two non-vanishing coordinates only). The determination of the remaining orbits of order 120 is then based on the results obtained so far.

Before proceeding, we recall that the $Q_i$ ($i = 1 \ldots 56$) label the $I_h$-inequivalent orbits of Dunlap and Zope and that the $A_i$ denote the corresponding indexed ones, both for the ideal case ($a_0 = 0.7042$) and for the standard one ($a_0 = 1$), as discussed in §3.

### 6.1. Indexing the orbits of order 60

A vanishing coordinate is left invariant by any scaling along the corresponding axis. Therefore only scalings along the two other orthogonal axes possibly occur for the positions belonging to orbits of order 60. According to Table 1 of Dunlop and Zope, 0 is the $z$ coordinate of $Q_1$ (for $C_{60}$), $Q_3$, $Q_4$ (for $C_{240}$), and $Q_5$, $Q_6$, $Q_7$ (for $C_{540}$). In all the other cases: $Q_{17}, \ldots, Q_{20}$ (for $C_{960}$), $Q_{31}, \ldots, Q_{35}$ (for $C_{1500}$) and $Q_{51}, \ldots, Q_{56}$ for $C_{2160}$ one has $y = 0$.

Therefore one tries to find scaling factors which relate the positions $Q_3$ to $Q_7$ to $A_1[9] = 0.7042(3\tau, 1, 0)$ and all the other ones to $A_1[1] = 0.7042(1, 0, 3\tau)$, where [1] and [9] refer to the successive order in which the vertices of $C_{60}$ are listed in Tables A.4 and A.5 of Wardman's PhD thesis. The result for the shells involved is listed in Table 4.

As $A_1[1]$ and $A_1[9]$ are related by cyclic permutation of their coordinates according to an icosahedral group element of order 3, it is very simple to express the orbits $A_3, \ldots, A_7$ in terms of crystallographic scalings from $A_1[1]$ instead of from $A_1[9]$ as in Table 4. For example the orbits $A_3$, $A_4$ are related to $A_1[1]$ by

$$X_2Z_2A_1[1] = [4, 0, 0, 2, 0, 0], \quad X_4Z_2A_1[1] = [5, 0, 0, 1, 0, 0]. \tag{10}$$

Accordingly all orbits of order 60 are related to one single position of $C_{60}$. As shown further on, this is true for all the icosahedral orbits of the whole series.

**Table 5**
$C_{60}$ polyhedra with hexagonal edges decorated by positions of generators of order 60 (standard case $a_0 = 1$).

| Shell polyhedron | Number of positions (orbits of order 60) | Pentagonal edges $e_p$ | Hexagonal edges $e_h$ |
|---|---|---|---|
| $C_{60}$ | 1 | 2 | 2 |
| $C_{240}$ | 2 | 2 | 8 |
| $C_{540}$ | 3 | 2 | 14 |
| $C_{960}$ | 4 | 2 | 20 |
| $C_{1500}$ | 5 | 2 | 26 |
| $C_{2160}$ | 6 | 2 | 32 |

One verifies the validity of the ideal positions indexed as indicated in Table 4 by comparison with the computed ones, where in some cases a rescaling of a few per cent was applied to individual computed orbits for getting a better global fitting between the computed positions and the indexed (ideal) ones. Examples are shown in Figs. 2 to Fig. 6. Moreover, these positions allow the definition of standard polyhedra having regularity properties summarized in Table 5. The general situation is illustrated in Fig. 3 for the $C_{960}$ fullerene.

In all fullerene shells the positions generating by $I_h$ the orbits of order 60 define polyhedra with the same number of vertices, edges and faces ($V$ $E$ $F$) = (60 90 32) and equal pentagonal edges ($e_p = 2a_0$). They differ in the length of the hexagonal edges which are decorated by positions at alternating distances $2a_0$ and $4a_0$. In the order-60 case, the number of inequivalent positions is $n$, thus equal to the successive numbering of the shells (see Table 5).

From the positions along the $x$ axis of these decorated polyhedra, oriented according to the icosahedral twofold axes, one can deduce corresponding $X_k$ scaling relations. So, for example, in the $C_{960}$ case, for the positions at distances 10, 8, 4 and 2 from the $y$ axis one finds scalings $X_{10}$, $X_8$, $X_4$, $X_2$ relating the common position $Z_4A_1[1] = \frac{1}{2}[13, 0, 0, 11, 0, 0]$ to the corresponding orbits $A_{19}, A_{20}, A_{18}, A_{17}$:

$$\begin{aligned} A_{17} &= X_2Z_4A_1[1] = [7, 0, 0, 5, 0, 0], \\ A_{18} &= X_4Z_4A_1[1] = [8, 0, 0, 4, 0, 0], \\ A_{19} &= X_{10}Z_4A_1[1] = [11, 0, 0, 1, 0, 0], \\ A_{20} &= X_8Z_4A_1[1] = [10, 0, 0, 2, 0, 0], \end{aligned} \tag{11}$$

implying the additional scaling relations (see Fig. 3)

$$A_{19} = X_5A_{17}, \quad A_{20} = X_4A_{17}, \quad A_{18} = X_2A_{17}. \tag{12}$$

### 6.2. Indexing the orbits of order 120

Before proceeding with the indexing of the elements belonging to the orbits of order 120, it is convenient to get a general view of the computed positions with respect to the ideal structure of the elements of order 60, derived in the preceding subsection. In all fullerene shells one finds a similar situation, illustrated here in Fig. 3 for $C_{960}$, where the computed nearest neighbours inside the hexagonal face of $C_{960}$ have been drawn connected. In a view along the twofold axis one sees that these positions form (approximately) a honeycomb net and are arranged along lines parallel to the $x$ axis. This allows one to deduce, as in the case discussed in the previous subsection, the expected $X_k$ scalings between aligned positions, starting from 60-order positions, turned by $2\pi/5^\circ$ from the previous determined ones along the $x$ axis.

For example, the positions belonging to the orbits $A_{11}, A_{12}, A_{14}$ are at aligned distances from the $y$ axis which are 1/11, 5/11 and 7/11, respectively, of the $y$ coordinate of $A_{19}[59] = [11, 0, 1, 0, 0, 0]$ (of order 60). Applying to this position corresponding scaling transformations one computes the indices of these positions:

$$\begin{aligned} A_{11}[61] &= X_{1/11}[11, 0, 1, 0, 0, 0] \\ &= [6, 0, 1, 5, 0, 0] \\ A_{12}[79] &= X_{5/11}[11, 0, 1, 0, 0, 0] \\ &= [8, 0, 1, 3, 0, 0] \\ A_{14}[53] &= X_{7/11}[11, 0, 1, 0, 0, 0] \\ &= [9, 0, 1, 2, 0, 0]. \end{aligned} \tag{13}$$

In a similar way from $A_{20}[55] = [10, 0, 2, 0, 0, 0]$ and $A_{17}[59] = [7, 0, 5, 0, 0, 0]$ one finds the generators of the remaining orbits:

$$\begin{aligned} A_{13}[35] &= X_{1/5}[10, 0, 2, 0, 0, 0] \\ &= [6, 0, 2, 4, 0, 0] \\ A_{16}[118] &= X_{2/5}[10, 0, 2, 0, 0, 0] \\ &= [7, 0, 2, 3, 0, 0] \\ A_{15}[18] &= X_{1/7}[7, 0, 5, 0, 0, 0] \\ &= [4, 0, 5, 3, 0, 0]. \end{aligned} \tag{14}$$

Finally, all the $I_h$ orbits of the fullerenes $C_{60}$, $C_{240}$, $C_{540}$, $C_{960}$, $C_{1500}$, $C_{2160}$ have been determined. The procedure is illustrated in Fig. 4 for the $C_{1500}$ fullerene, where the related order-120 positions are shown along the same blue line. As already mentioned, all are connected by crystallographic scalings to one single position, say $A_1[1] = [2, 0, 0, 1, 0, 0]$, and eventually also to the generator [1,0,0,0,0,0] of the icosahedron. In each shell, as already mentioned, all nearest neighbours are at the same distance $2a_0$. An overview of the 56 inequivalent indexed positions is reported in Table 6, to be compared with Table 1 of Dunlap and Zope for the computed carbon positions.

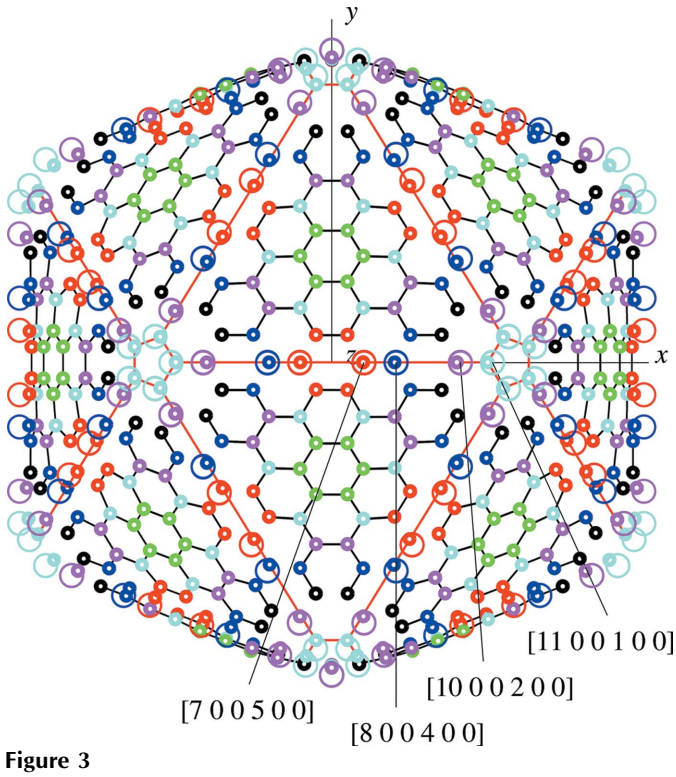


**Figure 3**
$C_{960}$ fullerene in a view along the icosahedral twofold axis. The indices of inequivalent positions of order 60 (large circles), occurring along the $x$ axis, are obtained by crystallographic scalings from the icosahedral vertex at [120000] and are compared with positions computed by Dunlap and Zope (filled circles of correspondingly same colour). The additional computed positions of orbits of order 120 form a honeycomb net inside the hexagonal faces (delimited by red lines).

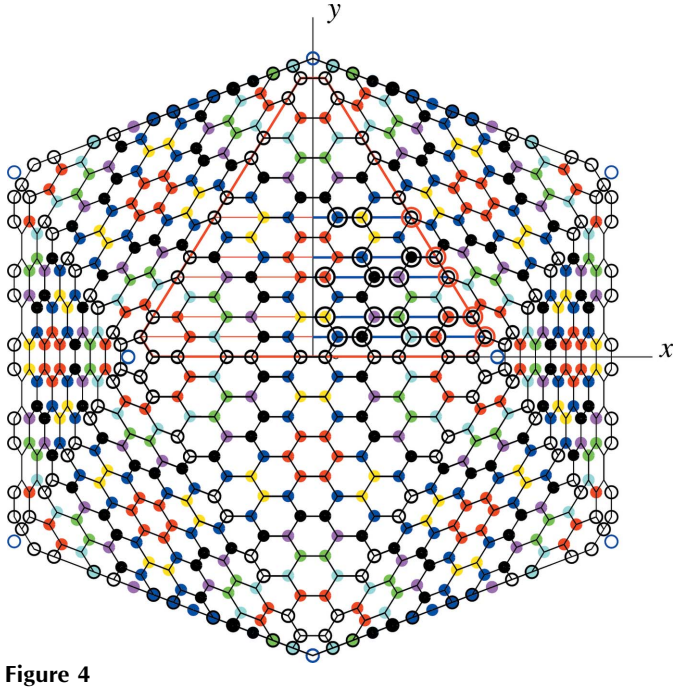


**Figure 4**
$C_{1500}$ fullerene. The positions of the orbits of order 60 are along the sides of the hexagonal faces (one face is delimited by a red line). The five inequivalent positions of order-60 orbits along the right-hand side of this face are marked by large circles and so also the additional 15 inequivalent positions which allow one to generate the orbits of order 120, obtained by crystallographic scaling from the order-60 positions aligned parallel to the $x$ axis and connected by a blue line.

**Table 6**
Inequivalent indexed positions in standard icosahedral fullerenes of the $C_{60}$ series.

| Fullerene | Orbit | Order | Indexed position |
|---|---|---|---|
| $C_{60}$ | $A_1$ | 60 | [0,0,0,0,2,1] |
| $C_{240}$ | $A_2$ | 120 | [1,3,0,0,0,2] |
| | $A_3$ | 60 | [0,4,0,0,0,2] |
| | $A_4$ | 60 | [0,5,0,0,0,1] |
| $C_{540}$ | $A_5$ | 60 | [7,0,0,2,0,0] |
| | $A_6$ | 60 | [5,4,0,0,0,0] |
| | $A_7$ | 60 | [0,8,0,0,0,1] |
| | $A_8$ | 120 | [6,0,2,1,0,0] |
| | $A_9$ | 120 | [1,0,3,5,0,0] |
| | $A_{10}$ | 120 | [3,2,0,0,0,4] |
| $C_{960}$ | $A_{11}$ | 120 | [6,0,1,5,0,0] |
| | $A_{12}$ | 120 | [8,0,1,3,0,0] |
| | $A_{13}$ | 120 | [6,0,2,4,0,0] |
| | $A_{14}$ | 120 | [9,0,1,2,0,0] |
| | $A_{15}$ | 120 | [5,0,3,4,0,0] |
| | $A_{16}$ | 120 | [7,0,2,3,0,0] |
| | $A_{17}$ | 60 | [7,0,0,5,0,0] |
| | $A_{18}$ | 60 | [8,0,0,4,0,0] |
| | $A_{19}$ | 60 | [11,0,0,1,0,0] |
| | $A_{20}$ | 60 | [10,0,0,2,0,0] |
| $C_{1500}$ | $A_{21}$ | 120 | [7,0,2,6,0,0] |
| | $A_{22}$ | 120 | [12,0,1,2,0,0] |
| | $A_{23}$ | 120 | [8,0,1,6,0,0] |
| | $A_{24}$ | 120 | [9,0,1,5,0,0] |
| | $A_{25}$ | 120 | [9,0,2,4,0,0] |
| | $A_{26}$ | 120 | [10,0,2,3,0,0] |
| | $A_{27}$ | 120 | [11,0,1,3,0,0] |
| | $A_{28}$ | 120 | [6,0,5,4,0,0] |
| | $A_{29}$ | 120 | [7,0,5,3,0,0] |
| | $A_{30}$ | 120 | [8,0,3,4,0,0] |
| | $A_{31}$ | 60 | [11,0,0,4,0,0] |
| | $A_{32}$ | 60 | [10,0,0,5,0,0] |
| | $A_{33}$ | 60 | [13,0,0,2,0,0] |
| | $A_{34}$ | 60 | [14,0,0,1,0,0] |
| | $A_{35}$ | 60 | [8,0,0,7,0,0] |
| $C_{2160}$ | $A_{36}$ | 120 | [9,0,2,7,0,0] |
| | $A_{37}$ | 120 | [10,0,2,6,0,0] |
| | $A_{38}$ | 120 | [12,0,2,4,0,0] |
| | $A_{39}$ | 120 | [13,0,2,3,0,0] |
| | $A_{40}$ | 120 | [14,0,1,3,0,0] |
| | $A_{41}$ | 120 | [15,0,1,2,0,0] |
| | $A_{42}$ | 120 | [11,0,1,6,0,0] |
| | $A_{43}$ | 120 | [12,0,1,5,0,0] |
| | $A_{44}$ | 120 | [9,0,1,8,0,0] |
| | $A_{45}$ | 120 | [8,0,4,6,0,0] |
| | $A_{46}$ | 120 | [9,0,4,5,0,0] |
| | $A_{47}$ | 120 | [10,0,3,5,0,0] |
| | $A_{48}$ | 120 | [11,0,3,4,0,0] |
| | $A_{49}$ | 120 | [8,0,3,7,0,0] |
| | $A_{50}$ | 120 | [7,0,5,6,0,0] |
| | $A_{51}$ | 60 | [10,0,0,8,0,0] |
| | $A_{52}$ | 60 | [11,0,0,7,0,0] |
| | $A_{53}$ | 60 | [14,0,0,4,0,0] |
| | $A_{54}$ | 60 | [13,0,0,5,0,0] |
| | $A_{55}$ | 60 | [16,0,0,2,0,0] |
| | $A_{56}$ | 60 | [17,0,0,1,0,0] |

## 7. The icosahedral $C_{60}$ onion

The 56 inequivalent indexed positions listed in Table 6, which generate the multishells formed by the six first icosahedral fullerenes $C_{60}$, $C_{240}$, $C_{540}$, $C_{960}$, $C_{1500}$ and $C_{2160}$ of the $C_{60}$ series, permit an algorithmic characterization whose validity can be extended to any integral value $n = 1, 2, \ldots, \infty$. In this way one can consider the whole $C_{60}$ series as a single molecular onion: the $C_{60}$ *onion*.

The $C_{60}$ onion is, accordingly, a space-filling one-parameter ($a_0$) discrete multishell structure with icosahedral symmetry, where, starting from $C_{60}$ (as a first shell), each successive other shell is an indexed fullerene (with the shape of a truncated icosahedron) obeying the given algorithm.

The aim of this section is to elucidate structural properties of the newly defined $C_{60}$ onion and to formulate the algorithm for the derivation of the $I_h$-inequivalent positions.

The properties depend, in general, on the parity of the shell number $n$. The odd and even cases are parametrized according to

$$n = n_{\rm odd} = 2j - 1 \text{ and } n = n_{\rm even} = 2j, \quad j = 1, 2, \ldots, \infty. \tag{15}$$

### 7.1. Topological properties

For a given shell, the number of inequivalent positions belonging to the orbit of order 60 is equal to the shell number $n$. For the orbits of order 120 the number of required positions depends on the parity of $n$:

$$N_{60} = n, \quad N_{120}^{\rm odd} = (j-1)(2j-1),$$
$$N_{120}^{\rm even} = j(2j-1), \quad j = 1, 2, \ldots, \infty. \tag{16}$$

As already mentioned, the number of pentagonal faces is always $f_{\rm p} = 12$, that of hexagonal faces in the truncated icosahedra is $f_6 = 20$ (which is not the number of hexagonal faces in each of the $n$th-shell fullerene, for $n > 1$).

One verifies the validity of these relations for the fullerenes considered by Dunlap and Zope (from $C_{60}$ to $C_{2160}$) and for the additional one $C_{2940}$ mentioned by Wardman, which occurs as the seventh shell ($n = 7$).

### 7.2. Geometrical characterization

The shells are truncated icosahedra in the same orientation, with equal pentagonal faces and honeycomb hexagons with the same edge length: $e_{\rm p} = e_{\rm h}$. The triangular face of the icosahedron of the shell $n$ has an edge of length $e_I$. The parallel set of these faces cuts the corresponding threefold axis at $h_I = nh_0$:

$$e_{\rm p} = e_{\rm h} = 2a_0, \quad e_I = 6na_0, \quad h_I = nh_0, \quad h_0 = 3^{1/2}\tau^2, \tag{17}$$

with $\tau$ the golden number. On each icosahedral edge $e_I$ there are $2n$ positions of order 60, in total therefore $60n$.

The positions of order 120 are inside the triangular icosahedral face and form a honeycomb net having hexagonal edges $e_{\rm h} = 2a_0$, equal to the pentagonal ones, and therefore there are $3n(n-1)$ on a given face and $60n(n-1)$ in total.

Accordingly, the total number of occupied positions is given by $60n + 60n(n-1) = 60n^2$. This geometrical characterization is summarized in Tables 7 and 8.

### 7.3. Caspar–Klug construction

The honeycomb net one finds in a planar face of the $n$th fullerene shell has as inside points the positions of order 120 and a boundary delimited by those of order 60. This suggests

that we should apply to the $C_{60}$ onion the construction devised by Caspar and Klug for the surface classification of icosahedral viruses (Caspar & Klug, 1962). A similar procedure to generate icosahedral fullerenes has been followed by Terrones *et al.* (2002).

As presented in Janner (2006), Caspar and Klug start from a planar honeycomb net and consider a planar hexagonal lattice with basis vectors $b_1$, $b_2$:

$$|b_1| = |b_2| = b_0, \quad b_1 b_2 = \tfrac{1}{2} b_0^2, \tag{18}$$

such that the honeycomb positions are lattice points with integral coordinates $z_1$ and $z_2$. The vertices of a triangular icosahedral face are put in coincidence with the lattice points $[0, 0], [h, k], [-k, h + k]$, respectively. The hexagonal basis vectors are along two sides of one face, which in the present case has a triangular edge $e_I = 6na_0$. The hexagonal edge of the honeycomb is $e_h = 2a_0 = b_0$. This implies for the shell $n$ the Caspar–Klug parameters $h = 3n$, $k = 0$ and the triangulation number $T = h^2 + hk + k^2 = Pf^2 = 9n^2$, thus $P = 1$ and co-factor $f = 3n$.

In order to fit these conventional parameters with the ones adopted so far, one first transforms the orthonormal basis $e = \{e_1, e_2, e_3\}$, oriented along the twofold axes, into one having an axis along a threefold direction. This can be achieved by a rotation $R(\beta)$ around the original $y$ direction, with $\tan\beta = \tau^2$:

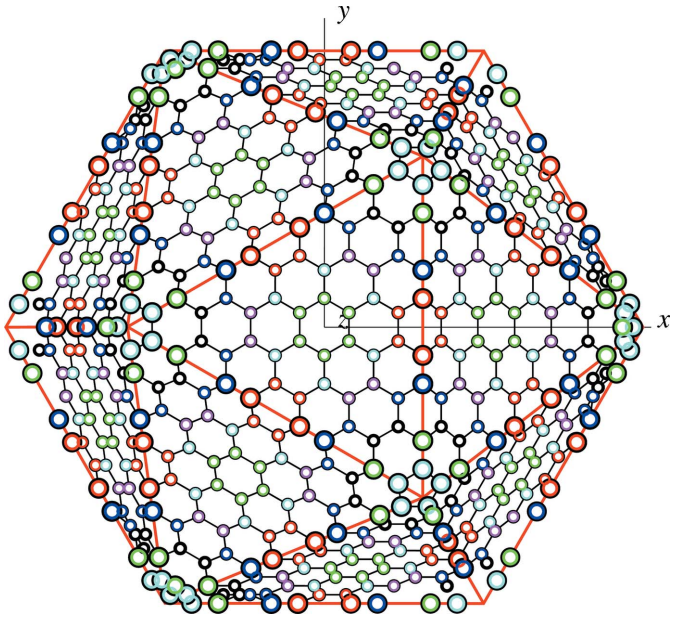


**Figure 5**
Shown is the fullerene $C_{960}$ in a view along an icosahedral threefold axis. Enhanced are the positions belonging to the orbits of order 60, occurring along the sides of the hexagonal faces (marked in red) delimiting the honeycomb net formed by the positions of the orbits of order 120.

**Table 7**
Geometry of the $n$th shell of the $C_{60}$ onion (for $a_0 = 1$).

| Icosahedron | | Truncated icosahedron | |
|---|---|---|---|
| Radius | $r_I = 3n(2+\tau)^{1/2}$ | $r_{max} = [(3n-2)^2 + (3n\tau)^2]^{1/2}$ | $r_{min} = (4 + 3n^2\tau^4)^{1/2}$ |
| Edge | $e_I = 6n$ | $e_h = 6n - 4$, $e_p = 2$ | Decorated, at alternative 2, 4 distances |
| Face | Triangular | Truncated triangle | Honeycomb with $e_h = 2$ |
| Axial face cut | $h_I = 3^{1/2} n\tau^2$ | $h_I = 3^{1/2} n\tau^2$ | |

**Table 8**
Occupied positions in the truncated icosahedra of the $C_{60}$ onion (for $a_0 = 1$).

| Shell $n$ | $n_{odd} = 2j - 1$ | | $n_{even} = 2j$ | |
|---|---|---|---|---|
| Positions | Order 60 | Order 120 | Order 60 | Order 120 |
| Total number | $2n$ | $3n(n-1)$ | $2n$ | $3n(n-1)$ |
| Inequivalent | $n$ | $(j-1)n$ | $n$ | $j(n-1)$ |

$$R(\beta) = \begin{pmatrix} \cos(\beta) & 0 & \sin(\beta) \\ 0 & 1 & 0 \\ -\sin(\beta) & 0 & \cos(\beta) \end{pmatrix} = \frac{1}{3^{1/2}} \begin{pmatrix} \tau - 1 & 0 & \tau \\ 0 & 3^{1/2} & 0 \\ -\tau & 0 & \tau - 1 \end{pmatrix}. \tag{19}$$

The coordinates $x, y, z$ of the twofold-symmetric system $e = \{e_1, e_2, e_3\}$ are then transformed by $R(-\beta)$ into the $x', y', z'$ ones of the rotated system $e' = \{e'_1, e'_2, e'_3\}$. In particular for the $\mathbb{Z}$ module $\Lambda_{ico}$ of equation (4) one has

$$\begin{aligned}
a_1 &= a_0(1, 0, \tau)_e = a_0(-2/3^{1/2}, 0, \tau^2/3^{1/2})_{e'}, \\
a_2 &= a_0(\tau, 1, 0)_e = a_0(1/3^{1/2}, 1, \tau^2/3^{1/2})_{e'}, \\
a_3 &= a_0(0, \tau, 1)_e = a_0(-\tau/3^{1/2}, \tau, (\tau-1)/3^{1/2})_{e'}, \\
a_4 &= a_0(-1, 0, \tau)_e = a_0(-2\tau/3^{1/2}, 0, (-\tau+1)/3^{1/2})_{e'}, \\
a_5 &= a_0(0, -\tau, 1)_e = a_0(-\tau/3^{1/2}, -\tau, (\tau-1)/3^{1/2})_{e'}, \\
a_6 &= a_0(\tau, -1, 0)_e = a_0(1/3^{1/2}, -1, \tau^2/3^{1/2})_{e'}.
\end{aligned} \tag{20}$$

It is, therefore, natural to choose as reference the face with icosahedral vertices along $a_1, a_2, a_6$ perpendicular to [110001], instead of that perpendicular to [111000] considered in Janner (2006). The result of this reorientation is shown in Fig. 5 for the fullerene $C_{960}$. An enlarged view of the reference face of the $C_{2160}$ fullerene can be seen in Fig. 6, where one has now the choice

$$b_1 = (a_2 - a_1) \text{ and } b_2 = (a_6 - a_1). \tag{21}$$

One then indicates the occupied fullerene positions of this face in terms of $z_1$ and $z_2$ coordinates.

### 7.4. The algorithm

Considered is the icosahedral triangular face perpendicular to the direction $a_1 + a_2 + a_6 = [110001]$ of the fullerene $C_{60n^2}$ forming the shell $n$ of the $C_{60}$ onion.

The Caspar–Klug hexagonal planar lattice $\Lambda_{CK}$ has basis vectors $b_1 = a_0[\bar{1}10000]$, $b_2 = a_0[\bar{1}00001]$, as indicated in

equation (21), and origin at the icosahedral vertex $V_1(n) = a_0[3n, 0, 0, 0, 0, 0]$.

The orbits of order 60 are generated from positions situated on icosahedral edges. The $n$ inequivalent ones can be chosen at positions defined as

$$nP_{z,0} = V_1(n) + zb_1 = [3n - z, z, 0, 0, 0, 0], \quad z = 1, 2, \ldots, z_{\max}, \quad z \neq 0 \bmod 3, \tag{22}$$

where

$$z_{\max} = \begin{cases} 3j - 2 \text{ if } n_{\text{odd}} = 2j - 1, \\ 3j - 1 \text{ if } n_{\text{even}} = 2j. \end{cases} \tag{23}$$

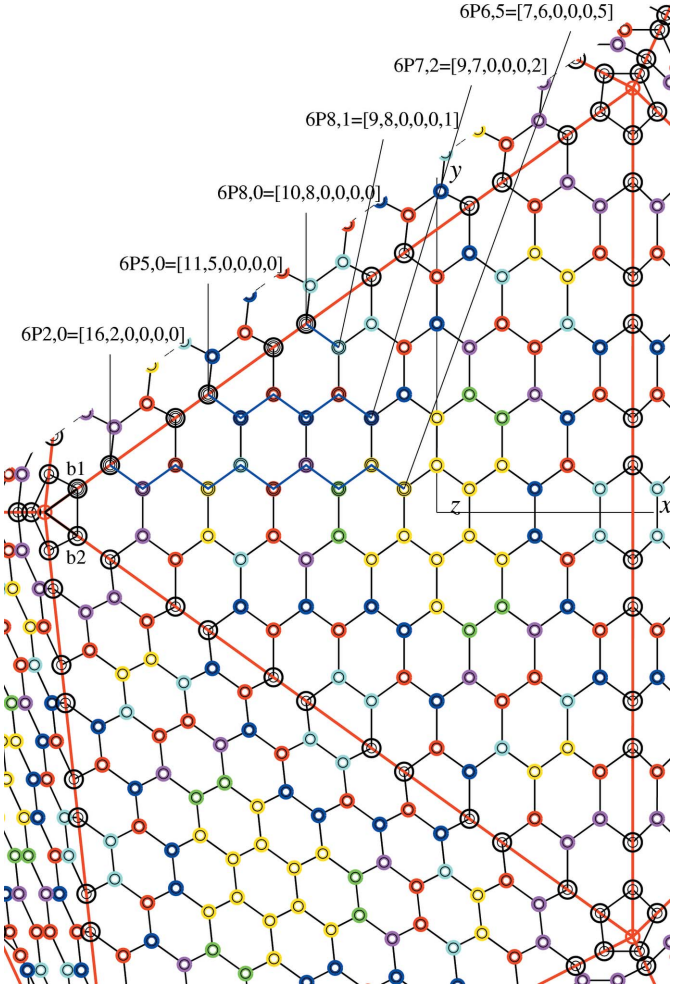


**Figure 6**
Enlarged view of the hexagonal face of the fullerene $C_{2160}$ belonging to the icosahedral triangular one with vertices at $V_1 = [100000]$, $V_2 = [010000]$ and $V_6 = [000001]$. The indexed positions of this fullerene have been derived on the basis of the algorithm indicated in the text and based on the Caspar–Klug construction. Along the side $V_1$–$V_2$ the six inequivalent positions of the order-60 orbits are marked by large circles and labelled as $6P_{z,0}$ according to their coordinate with respect to the hexagonal planar Caspar–Klug lattice, with the origin at $V_1$ and basis vectors $b_1$, $b_2$ shown as thick black segments. From these marked positions, along a zigzag line delimiting hexagons of the honeycomb net, one finds the 15 inequivalent order-120 positions, also encircled and labelled as $6P_{z_1,z_2}$, with $z_1$, $z_2$ their planar lattice coordinates.

The orbits of order 120 are generated from positions at the honeycomb points inside the triangular face and can be parametrized as

$$nP_{z_1,z_2} = V_1(n) + z_1b_1 + z_2b_2 = [3n - z_1 - z_2, z_1, 0, 0, 0, z_2], \quad z_1 \neq 0, \quad z_2 \neq 0, \quad z_1 \neq z_2, \tag{24}$$

forming a zigzag pattern starting from order-60 positions $nP_{z,0}$. Both obey the relations valid for $nPz_1, z_2$:

$$z_2 + 1 \leq z_1 \leq z_{\max}\, z_2 = 1, \ldots, (n - 1), \quad z_1 - z_2 \neq 0 \bmod 3 \tag{25}$$

where $z_{\max}$ is as above in equation (23) (see Fig. 6 for $n = 6$). Note that these positions generate the orbits, but are not all $I_h$-inequivalent.

The 56 inequivalent positions obtained by applying the algorithm to the first six shells of the $C_{60}$ onion are reported in Table 9. These positions correspond to those of Table 6. For a given orbit, the indices of the positions listed in the two tables are, in general, not the same.

## 8. Strong correlation

Each individual shell and the whole infinitely large $C_{60}$ onion molecule are generated by the icosahedral group $I_h$ from positions mutually related by crystallographic transformations. These are either scalings (as in §6) or lattice translations (as in §7). Note that, in the last case, the planar hexagonal lattice translations are combined with the translations (along a threefold axis) connecting the various shells. Remarkably enough, these translations are similar to lattice translations as they are all multiples of a fundamental one, which in the present case is the distance from the centre of a hexagonal face of $C_{60}$. These positions, even if inequivalent, are not independent but all correlated.

Furthermore, as all positions together depend on a single parameter only ($a_0$), the structure is said to be *strongly correlated*. This concept has been introduced in a series of previous articles on axial-symmetric proteins. [See, in particular, Janner (2005) which deals with protein–DNA (or RNA) complexes.] Usually, when speaking of strong correlation, electrons are intended and not, as here, atomic positions.

In §6 the correlating transformations are crystallographic scalings, whereas in §7 they are lattice translations. In fact, the scalings considered in §6 can be transformed into the translations in §7 and both types can be transformed into one another. This underlines their common crystallographic nature.

To give an example: starting from the $C_{60}$ position $A_1[1] = [2, 0, 0, 1, 0, 0] = (1, 0, 3\tau)_e$, the lattice translation $t_k = k[1, 0, 0, \overline{1}, 0, 0] = (2k, 0, 0)_e$ is equivalent with the crystallographic scaling $X_{1+2k}$:

**Table 9**
Inequivalent indexed positions in the first six shells of the $C_{60}$ onion derived according to the given algorithm (icosahedral parameter $a_0 = 1$).

| Shell $n$ | Position | Orbit |
|---|---|---|
| 1 ($C_{60}$) | $1P_{1,0} = [2, 1, 0, 0, 0, 0]$ | $A_1$ |
| 2 ($C_{240}$) | $2P_{1,0} = [5, 1, 0, 0, 0, 0]$ | $A_4$ |
| | $2P_{2,0} = [4, 2, 0, 0, 0, 0]$ | $A_3$ |
| | $2P_{2,1} = [3, 2, 0, 0, 0, 1]$ | $A_2$ |
| 3 ($C_{540}$) | $3P_{1,0} = [8, 1, 0, 0, 0, 0]$ | $A_7$ |
| | $3P_{2,0} = [7, 2, 0, 0, 0, 0]$ | $A_5$ |
| | $3P_{4,0} = [5, 4, 0, 0, 0, 0]$ | $A_6$ |
| | $3P_{2,1} = [6, 2, 0, 0, 0, 1]$ | $A_8$ |
| | $3P_{3,1} = [5, 3, 0, 0, 0, 1]$ | $A_9$ |
| | $3P_{3,2} = [4, 3, 0, 0, 0, 2]$ | $A_{10}$ |
| 4 ($C_{960}$) | $4P_{1,0} = [11, 1, 0, 0, 0, 0]$ | $A_{19}$ |
| | $4P_{2,0} = [10, 2, 0, 0, 0, 0]$ | $A_{20}$ |
| | $4P_{4,0} = [8, 4, 0, 0, 0, 0]$ | $A_{18}$ |
| | $4P_{5,0} = [7, 5, 0, 0, 0, 0]$ | $A_{17}$ |
| | $4P_{2,1} = [9, 2, 0, 0, 0, 1]$ | $A_{14}$ |
| | $4P_{3,1} = [8, 3, 0, 0, 0, 1]$ | $A_{12}$ |
| | $4P_{3,2} = [7, 3, 0, 0, 0, 2]$ | $A_{16}$ |
| | $4P_{4,2} = [6, 4, 0, 0, 0, 2]$ | $A_{13}$ |
| | $4P_{4,3} = [5, 4, 0, 0, 0, 3]$ | $A_{15}$ |
| | $4P_{5,1} = [6, 5, 0, 0, 0, 1]$ | $A_{11}$ |
| 5 ($C_{1500}$) | $5P_{1,0} = [14, 1, 0, 0, 0, 0]$ | $A_{34}$ |
| | $5P_{2,0} = [13, 2, 0, 0, 0, 0]$ | $A_{33}$ |
| | $5P_{4,0} = [11, 4, 0, 0, 0, 0]$ | $A_{31}$ |
| | $5P_{5,0} = [10, 5, 0, 0, 0, 0]$ | $A_{32}$ |
| | $5P_{7,0} = [8, 7, 0, 0, 0, 0]$ | $A_{35}$ |
| | $5P_{2,1} = [12, 2, 0, 0, 0, 1]$ | $A_{22}$ |
| | $5P_{3,1} = [11, 3, 0, 0, 0, 1]$ | $A_{27}$ |
| | $5P_{3,2} = [10, 3, 0, 0, 0, 2]$ | $A_{26}$ |
| | $5P_{4,2} = [9, 4, 0, 0, 0, 2]$ | $A_{25}$ |
| | $5P_{4,3} = [8, 4, 0, 0, 0, 3]$ | $A_{30}$ |
| | $5P_{5,3} = [7, 5, 0, 0, 0, 3]$ | $A_{29}$ |
| | $5P_{5,4} = [6, 5, 0, 0, 0, 4]$ | $A_{28}$ |
| | $5P_{5,1} = [9, 5, 0, 0, 0, 1]$ | $A_{24}$ |
| | $5P_{6,1} = [8, 6, 0, 0, 0, 1]$ | $A_{23}$ |
| | $5P_{6,2} = [7, 6, 0, 0, 0, 2]$ | $A_{21}$ |
| 6 ($C_{2160}$) | $6P_{1,0} = [17, 1, 0, 0, 0, 0]$ | $A_{56}$ |
| | $6P_{2,0} = [16, 2, 0, 0, 0, 0]$ | $A_{55}$ |
| | $6P_{4,0} = [14, 4, 0, 0, 0, 0]$ | $A_{53}$ |
| | $6P_{5,0} = [13, 5, 0, 0, 0, 0]$ | $A_{54}$ |
| | $6P_{7,0} = [11, 7, 0, 0, 0, 0]$ | $A_{52}$ |
| | $6P_{8,0} = [10, 8, 0, 0, 0, 0]$ | $A_{51}$ |
| | $6P_{2,1} = [15, 2, 0, 0, 0, 1]$ | $A_{41}$ |
| | $6P_{3,1} = [14, 3, 0, 0, 0, 1]$ | $A_{40}$ |
| | $6P_{3,2} = [13, 3, 0, 0, 0, 2]$ | $A_{39}$ |
| | $6P_{4,2} = [12, 4, 0, 0, 0, 2]$ | $A_{38}$ |
| | $6P_{4,3} = [11, 4, 0, 0, 0, 3]$ | $A_{48}$ |
| | $6P_{5,3} = [10, 5, 0, 0, 0, 3]$ | $A_{47}$ |
| | $6P_{5,4} = [9, 5, 0, 0, 0, 4]$ | $A_{46}$ |
| | $6P_{6,4} = [8, 6, 0, 0, 0, 4]$ | $A_{45}$ |
| | $6P_{6,5} = [7, 6, 0, 0, 0, 5]$ | $A_{50}$ |
| | $6P_{5,1} = [12, 5, 0, 0, 0, 1]$ | $A_{43}$ |
| | $6P_{6,1} = [11, 6, 0, 0, 0, 1]$ | $A_{42}$ |
| | $6P_{6,2} = [10, 6, 0, 0, 0, 2]$ | $A_{37}$ |
| | $6P_{7,2} = [9, 7, 0, 0, 0, 2]$ | $A_{36}$ |
| | $6P_{7,3} = [8, 7, 0, 0, 0, 3]$ | $A_{49}$ |
| | $6P_{8,1} = [9, 8, 0, 0, 0, 1]$ | $A_{44}$ |

$$\begin{aligned} A_1[1] + t_k &= (1, 0, 3\tau) + (2k, 0, 0) \\ &= [2, 0, 0, 1, 0, 0] + k[1, 0, 0, \bar{1}, 0, 0] \\ &= X_{1+2k}A_1[1] = X_{1+2k}(1, 0, 3\tau) = (1 + 2k, 0, 3\tau) \\ &= [2 + k, 0, 0, 1 - k, 0, 0]. \end{aligned} \quad (26)$$

It is also possible to formulate the algorithm (based above on lattice translations) in terms of crystallographic scalings. In this case, however, one has to select the positions in the hexagonal face of fullerenes in the twofold orientation, as in §6, instead of in a threefold orientation as in §7.

The strong correlation of the inequivalent positions suggests for the $C_{60}$ onion a larger point-group symmetry than the icosahedral group. The verification of this expectation is a goal beyond the aim of the present article. It is already now clear that this group cannot be orthogonal, because the positions involved have different radial distances from the centre of the molecule. Furthermore, neither the correlating translations are admitted, nor do the crystallographic scalings have a discrete structure.

## 9. Graphene sheets in $C_{60}$ onion and in graphite

Let us recall that graphene is a two-dimensional crystal formed by one sheet of graphite (Katsnelson, 2012) and has a honeycomb net structure.

The successive shells in the $C_{60}$ onion share the same icosahedral orientation, and so also that of their pentagonal and hexagonal faces. All the edges of the pentagons and of the hexagons of the honeycomb nets inside the hexagonal faces have equal length $2a_0$. The distance between successive hexagonal faces is $h_0$, as already derived in equation (17).

Moreover, the stacked honeycomb hexagons are in a centre-to-centre and vertex-to-vertex relation, as shown in Fig. 7 for the successive indexed fullerenes $C_{60}$, $C_{240}$, $C_{540}$, $C_{960}$, $C_{1500}$, $C_{2160}$, in a view along the $z$ axis (in the [110001] direction) and along the $y$ axis (perpendicular to it), respectively. In this figure, red lines indicate the sides of the triangular icosahedral faces involved and black circles mark the positions belonging to the orbits of order 60 and 120.

For $a_0 = 0.71$ Å one gets the indexed model of the carbon $C_{60}$ onion, with 1.42 Å for the C—C distance $d_g$, as in graphite and in graphene. It is then natural to compare the distances between graphene sheets in the $C_{60}$ onion ($h_0$) and in graphite ($h_g$) with respect to the common planar C—C distance $d_g = e_h$. One finds

$$h_0/e_h = 3^{1/2}\tau^2/2 = 2.267, \quad h_g/d_g = \frac{3.35}{1.42} = 2.359, \quad (27)$$

with a 4% difference between the ratios for the indexed model $C_{60}$ onion and for the experimental graphite. Note that the equal spacing between nested fullerenes was noticed by Kroto & McKay (1988). They also pointed out that this spacing ($1.42h_0/e_h$ = 3.22 Å) is *circa* the same as between sheets of graphite (3.35 Å) (Kroto & McKay, 1988).

As such, a difference between the two values is quite acceptable, because of the three different types of structures involved: experimental, computational and indexed model, which are intrinsically mutual approximations. A typical example is the different C—C distance computed by Dunlap and Zope for pentagonal and for hexagonal faces of $C_{60}$ indicated in equation (7).

If one takes the relation of equation (27) as significant for an indexed model of graphite, it would imply a strong correlation expressed by a relation between the $a$ and $c$ parameters of the hexagonal lattice of graphite:

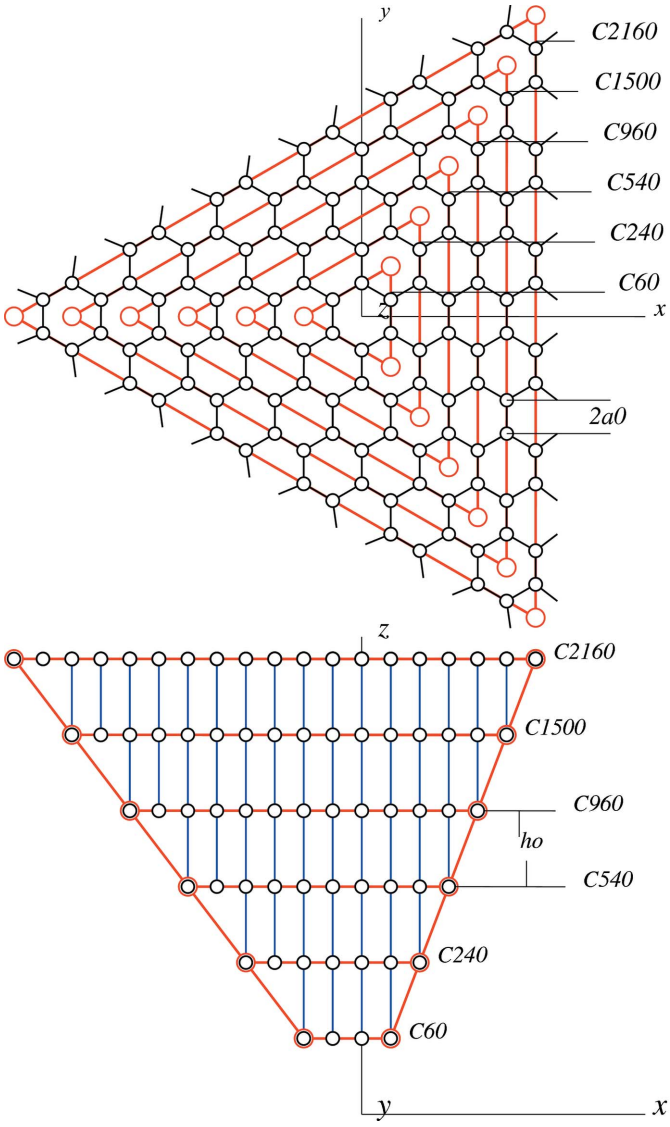


**Figure 7**
Set of faces of the $C_{60}$ onion viewed along the threefold [1,1,0,0,0,1] ($z$ axis) and perpendicular to this direction ($y$ axis) in the upper and lower parts, respectively. The black circles indicate positions belonging to the orbits involved. The distance between the sheets is $h_0 = 3^{1/2}\tau^2 a_0/2$. That between positions in the plane (sides of the honeycomb hexagons) is $2a_0$, which corresponds to the shortest C—C distance. The red lines indicate the icosahedral triangular faces delimiting the hexagonal ones of the fullerenes.

$$c = \tau^2 a = 6.43\ \text{Å}; \qquad (28)$$

to be compared with the experimental values of $a$ = 2.456 Å and $c$ = 6.708 Å. Again a 4% discrepancy is found.

Note that in graphite the hexagons of the graphene sheets are stacked in a centre-to-vertex relation and not centre-to-centre as in the $C_{60}$ onion (see Fig. 7).

Whether the relation between the model onion and graphite presented is accidental or relevant depends on the existence or not of a general meaningful context. The matter presented in the next section possibly represents the desired theoretical basis for such a context and for further future investigations. In any case, it is a fact that with increasing shell number the importance of the pentagonal faces with respect to the graphite-like hexagonal honeycomb ones strongly decreases.

**Table 10**
Structural parameters of the graphite model, with hexagonal lattice and Wyckoff positions 2$a$, 2$b$ of the space group $P6_3mc$ expressed in indices of the $\mathbb{Z}$ module $\Lambda_{ico}$ and components $x$, $y$, $z$ in the orthonormal basis $e'$ with $e'_3$ along the hexagonal axis (in the icosahedral threefold direction).

| Graphite model | Parameters | $P6_3mc$ | $\mathbb{Z}$ module $\Lambda_{ico}$ | $(x, y, z)_{e'}$ |
|---|---|---|---|---|
| Hexagonal lattice | $a$ | [100] | $[1\bar{2}0001]$ | $-3^{1/2}, -3, 0$ |
| | $b$ | [010] | $[\bar{2}10001]$ | $2(3)^{1/2}, 0, 0$ |
| | $c$ | [001] | [220002] | $0, 0, 2(3)^{1/2}\tau^2$ |
| Occupied positions | 2$a$ | [000] | [000000] | 0, 0, 0 |
| | | $[00\frac{1}{2}]$ | [110001] | $0, 0, (3)^{1/2}\tau^2$ |
| | 2$b$ | $[\frac{1}{3}\frac{2}{3}0]$ | $[\bar{1}00001]$ | $3^{1/2}, -1, 0$ |
| | | $[\frac{2}{3}\frac{1}{3}\frac{1}{2}]$ | [100002] | $0, -2, (3)^{1/2}\tau^2$ |

## 10. A one-parameter model of graphite

It is possible to define a structural model which has the same Euclidean symmetry as graphite and the same occupied Wyckoff positions 2$a$ and 2$b$ of the space group $P6_3mc$ and, at the same time, integral indices when expressed in the icosahedral $\mathbb{Z}$ module of equations (4) and (20).

In Table 10, the hexagonal lattice and the occupied Wyckoff positions of the space group $P6_3mc$ are expressed in integral indices of the $\mathbb{Z}$ module $\Lambda_{ico}$ and in components of the orthonormal basis $e' = \{e'_1, e'_2, e'_3\}$ with $e'_3$ along the hexagonal axis (parallel to an icosahedral threefold direction). This leads to a one-parameter ideal model of graphite, with $c = \tau^2 a$ instead of the two parameters of the experimental graphite ($a$ and $c$).

One can now look at the relation between carbon positions in the fullerenes of the $C_{60}$ onion and of the graphite model. Both ideal structures approximate the corresponding experimental (or computed) ones. Such a comparison requires a shift in origin, because the standard origin of $P6_3mc$ does not correspond to the centre of the $C_{60}$ onion, which is at the $\frac{1}{3}, \frac{2}{3}, 0$ position, corresponding to $[\bar{1}00001]$ (see Table 10).

Conversely, as one can see from Fig. 8, in the graphite-like interpretation of $C_{60}$ positions, the origin [000] of $P6_3mc$ has to be chosen at $[10000\bar{1}]$. Let us consider $C_{60}$ positions which correspond with the graphite-like positions $[0\,0\,\frac{1}{2}]$ and $[0\,1\,\frac{1}{2}]$, respectively, and the indices of the graphite-like position at $\frac{1}{3}, \frac{2}{3}, 0$:

$$\begin{aligned}
0\,0\,\tfrac{1}{2} &= 10000\bar{1} + \tfrac{1}{2}220002 = 210000\\
0\,1\,\tfrac{1}{2} &= 10000\bar{1} + \bar{2}10001 + \tfrac{1}{2}220002 = 020001\\
\bar{1}00001 &= \left(\frac{2}{3^{1/2}}, 0, -\frac{\tau^2}{3^{1/2}}\right) + \left(\frac{1}{3^{1/2}}, -1, \frac{\tau^2}{3^{1/2}}\right) = (3^{1/2}, -1, 0)\\
\left[\tfrac{1}{3}\tfrac{2}{3}0\right] &= \left(-\frac{1}{3^{1/2}}, -1, 0\right) + \left(\frac{4}{3^{1/2}}, 0, 0\right) = (3^{1/2}, -1, 0). \qquad (29)
\end{aligned}$$

So far for the $C_{60}$. Looking now at the graphite-like positions in the various shells of the $C_{60}$ onion (and thus at the full series

**Table 11**
Positions occurring in both the icosahedral model of the $C_{60}$ onion and in the one-parameter hexagonal model of graphite.

Parallel hexagonal faces of the onion shells are in one-to-one correspondence with graphite sheets. Two positions of $C_{240}$ are indicated in brackets because they do not fit with the space-group symmetry of graphite. See Fig. 8 for the first onion shell, the $C_{60}$ fullerene.

| $C_{60}$ onion | | | | One-parameter graphite | | |
|---|---|---|---|---|---|---|
| Fullerene | $I_h$ orbit | Order | Indices | $P6_3mc$ | Wyckoff position | Coordinates |
| $C_{60}$ | $A_1$ | 60 | 210000 | $00\frac{1}{2}$ | $2a$ | $0, 0, (3)^{1/2}\tau^2$ |
| | | | 020001 | $01\frac{1}{2}$ | $2a$ | $2(3)^{1/2}, 0, (3)^{1/2}\tau^2$ |
| | | | 100002 | $11\frac{1}{2}$ | $2a$ | $(3)^{1/2}, -3, (3)^{1/2}\tau^2$ |
| $C_{240}$ | $A_2$ | 120 | 320001 | 001 | $2a$ | $0, 0, 2(3)^{1/2}\tau^2$ |
| | | | 130002 | 011 | $2a$ | $2(3)^{1/2}, 0, 2(3)^{1/2}\tau^2$ |
| | | | (310002) | $(\frac{2}{3}\frac{1}{3}1)$ | | |
| | $A_3$ | 60 | 400002 | 101 | $2a$ | $-(3)^{1/2}, -3, 2(3)^{1/2}\tau^2$ |
| | $A_4$ | 60 | (500001) | $(\frac{2}{3}\frac{\bar{1}}{3}1)$ | | |
| $C_{540}$ | $A_5$ | 60 | 720000 | $\bar{1}\frac{\bar{5}}{3}\frac{3}{2}$ | $2b$ | $-3(3)^{1/2}, 1, 3(3)^{1/2}\tau^2$ |
| | $A_6$ | 60 | 540000 | $\bar{1}\bar{1}\frac{3}{2}$ | $2a$ | $-(3)^{1/2}, 3, 3(3)^{1/2}\tau^2$ |
| | $A_7$ | 60 | 800001 | $\frac{2}{3}\frac{\bar{5}}{3}\frac{3}{2}$ | $2b$ | $-4(3)^{1/2}, -2, 3(3)^{1/2}\tau^2$ |
| | $A_8$ | 120 | 620001 | $0\bar{1}\frac{3}{2}$ | $2a$ | $-2(3)^{1/2}, 0, 3(3)^{1/2}\tau^2$ |
| | $A_9$ | 120 | 510003 | $10\frac{3}{2}$ | $2a$ | $-(3)^{1/2}, -3, 3(3)^{1/2}\tau^2$ |
| | $A_{10}$ | 120 | 430002 | $00\frac{3}{2}$ | $2a$ | $0, 0, 3(3)^{1/2}\tau^2$ |
| ... | ... | ... | ... | ... | ... | ... |

of ideal fullerenes $C_{60}$, $C_{240}$, $C_{540}$, $C_{960}$, ...), one finds that all positions belonging to a parallel set of hexagonal faces of the odd shells ($C_{60}$, $C_{540}$ *etc.*) are at odd sheets ($A$) of the graphite model, whereas only half of the positions in the even shells ($C_{240}$, $C_{960}$ *etc.*) are at graphite-like positions of the even sheets ($B$).

This property means that the $C_{60}$ onion adopts the maximal possible graphite-like positions compatible with the orientation of the various shells imposed by the icosahedral symmetry $I_h$ of the whole ideal molecule. Moreover, the number of these positions increases with the increases in the shell number $n$.

A set of corresponding positions is given in Table 11, to be compared with the results of Table 1 of Dunlap and Zope and Tables 4 and 6 of this paper. All the examples given, and possible additional ones, can be computed in a similar way as indicated in equation (29).

## 11. Conclusion

As shown in this paper (and in a number of previous ones), molecular crystallography (which allows alternative approaches like affine extensions and rational scalings) reveals non-trivial structural relations hidden in the Euclidean description of the crystallographic structure.

Normally, the determination of these additional relations is based on a model structure derived from diffraction experiments. In the present case, the icosahedral fullerene models are obtained from a density-functional computation by Dunlap & Zope (2006) and the relations are derived here from crystallographic scalings applied to the fullerene structures, or alternatively by Wardman (2012) from a selection of point arrays constructed from affine extension of the icosahedral group $I_h$.

As already mentioned in §5, Wardman's main result is that her procedure simultaneously models different shells of a carbon onion (see her PhD thesis, p. 144).

In the alternative approach presented here, a similar result is represented by the single-parameter ($a_0$) dependency shown to occur in each fullerene of the $C_{60}$ series, in the infinitely large multishell molecular $C_{60}$ onion and the ideal graphite model. This implies in the three cases that all the atomic positions are mutually correlated, *i.e.* that these structures are *strongly correlated*. The correlation is also formulated in terms of an algorithm based on the construction devised by Caspar–Klug for the classification of icosahedral viruses (Caspar & Klug, 1962). This allows us to consider the $C_{60}$ onion as such, quite independently from how the defining algorithm is derived, and so also the model of the one-parameter ideal graphite.

It should be clear that the realm of fullerenes (and of icosahedral fullerenes, in particular) is much richer than discussed in this paper. For example, there is a different $C_{240}$ fullerene, also based on $C_{60}$, where all carbon positions belong to orbits of order 60 and are, therefore, situated on the hexagonal edges (Cárdenas *et al.*, 2012).

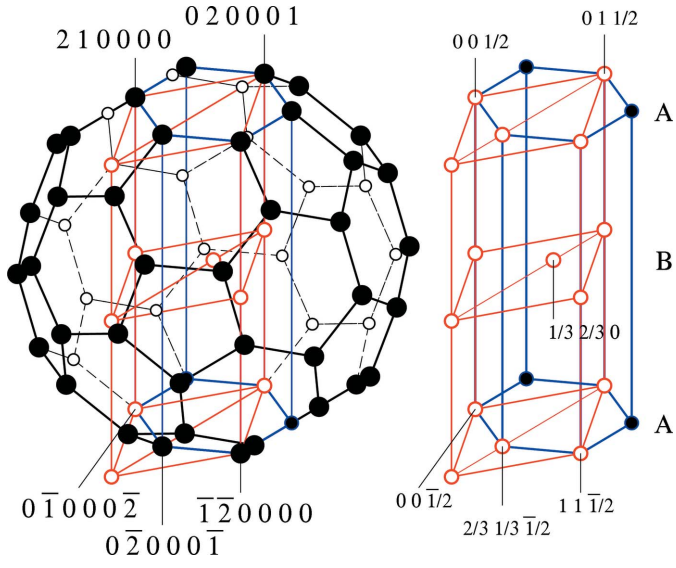


**Figure 8**
Comparison between the $C_{60}$ fullerene and a model of the graphite structure. The positions of the fullerene which belong to a parallel pair of hexagonal faces are at positions of the space group $P6_3mc$ of the graphite. This allows one to identify the icosahedral indexed carbon positions with their Wyckoff positions in the space group, implying a $c/a = \tau^2 \simeq 2.618$ relation deviating by about 4% from the value observed in graphite (6.708/2.456 = 2.731). The centre of the $C_{60}$ is at $\frac{1}{3}, \frac{2}{3}, 0$ of $P6_3mc$.

More has to be investigated further: in other fullerene series [already considered by Wardman (2012)], in icosahedral viruses (Keef *et al.*, 2013) and in complex intermetallics, as discussed by researchers of the Laboratory of Crystallography, ETH Zürich (Dshemuchadse *et al.*, 2013).

## APPENDIX *A*

Linear scaling transformations indicated in equation (5), expressed in the icosahedral basis $a$ of equation (4), with $k = n/m$ a fractional number:

$$X_k(a) = \frac{1}{2}\begin{pmatrix} k+1 & 0 & 0 & -k+1 & 0 & 0 \\ 0 & k+1 & 0 & 0 & 0 & k-1 \\ 0 & 0 & 2 & 0 & 0 & 0 \\ -k+1 & 0 & 0 & k+1 & 0 & 0 \\ 0 & 0 & 0 & 0 & 2 & 0 \\ 0 & k-1 & 0 & 0 & 0 & k+1 \end{pmatrix},$$

$$Y_k(a) = \frac{1}{2}\begin{pmatrix} 2 & 0 & 0 & 0 & 0 & 0 \\ 0 & k+1 & 0 & 0 & 0 & -k+1 \\ 0 & 0 & k+1 & 0 & -k+1 & 0 \\ 0 & 0 & 0 & 2 & 0 & 0 \\ 0 & 0 & -k+1 & 0 & k+1 & 0 \\ 0 & -k+1 & 0 & 0 & 0 & k+1 \end{pmatrix},$$

$$Z_k(a) = \frac{1}{2}\begin{pmatrix} k+1 & 0 & 0 & k-1 & 0 & 0 \\ 0 & 2 & 0 & 0 & 0 & 0 \\ 0 & 0 & k+1 & 0 & k-1 & 0 \\ k-1 & 0 & 0 & k+1 & 0 & 0 \\ 0 & 0 & k-1 & 0 & k+1 & 0 \\ 0 & 0 & 0 & 0 & 0 & 2 \end{pmatrix}. \qquad (30)$$

The stimulating comments of Professor Annalisa Fasolino, who also indicated publications on fullerene onions relevant for the present work, and the valuable improvements suggested by the referees are gratefully acknowledged.

## References

Bühl, M. & Hirsch, A. (2001). *Chem. Rev.* **101**, 1153–1183.
Calaminici, P., Carmona-Espindola, J., Geudtner, G. & Köster, A. M. (2012). *Int. J. Quantum Chem.* **112**, 3252–3255.
Cárdenas, C., Munoz, F., Munoz, M., Bernardin, A. & Fuentealba, P. (2012). *Phys. Chem. Chem. Phys.* **14**, 14810–14814.
Caspar, D. L. D. & Klug, A. (1962). *Cold Spring Harb. Symp. Quant. Biol.* **27**, 1–24.
Chung, F. & Sternberg, Sh. (1993). *Am. Scientist*, **81**, 56–71.
Dshemuchadse, J., Bigler, S., Simonov, A., Weber, T. & Steurer, W. (2013). *Acta Cryst.* B**69**, 238–248.
Dunlap, B. I. & Zope, R. R. (2006). *Chem. Phys. Lett.* **422**, 451–454.
Fleming, R. M., Hessen, B., Siegriest, T., Kortan, A. R., Marsh, P., Tycko, R., Dabbagh, G. & Haddon, R. C. (1992). *Fullerenes: Synthesis, Properties and Chemistry of Large Carbon Clusters*, ACS Symposium Series 481, edited by G. S. Hammond & V. J. Kuck, ch. 2, pp. 25–39. Washington DC: American Chemical Society.
Hadfield, A. T., Lee, W., Zhao, R., Oliveira, M. A., Minor, I., Rueckert, R. R. & Rossmann, M. G. (1997). *Structure*, **5**, 427–441.
Janner, A. (2005). *Acta Cryst.* D**61**, 269–277.
Janner, A. (2006). *Acta Cryst.* A**62**, 319–330.
Janner, A. (2013). *Acta Cryst.* A**69**, 151–163.
Katsnelson, M. I. (2012). *Graphene. Carbon in Two Dimensions.* Cambridge University Press.
Keef, T. & Twarock, R. (2009). *J. Math. Biol.* **59**, 287–313.
Keef, T., Wardman, J. P., Ranson, N. A., Stockley, P. G. & Twarock, R. (2013). *Acta Cryst.* A**69**, 140–150.
Kroto, H. W., Heath, J. R., O'Brien, S. C., Curl, R. F. & Smalley, R. E. (1985). *Nature (London)*, **318**, 162–163.
Kroto, H. W. & McKay, K. (1988). *Nature (London)*, **331**, 328–331.
Maiti, A., Brabec, C. J. & Bernholc, J. (1993). *Phys. Rev. Lett.* **70**, 3023–3026.
Terrones, M., Terrones, G. & Terrones, H. (2002). *Struct. Chem.* **13**, 373–384.
Wardman, J. P. (2012). PhD thesis, University of York, England.